Template-independent genome editing and repairing correct frameshift disease *in vivo*

Lian Liu[1,2,9], Kuan Li[1,3,9], Linzhi Zou[1,2,9], Hanqing Hou[1,2], Qun Hu[1,2], Shuang Liu[1,2], Shufeng Wang[1,2], Yangzhen Wang[1,2], Jie Li[1,2], Chenmeng Song[1,2], Jiaofeng Chen[1,2], Changri Li[4], Haibo Du[5], Jun-Liszt Li[6,7], Fangyi Chen[4], Zhigang Xu[5], Wenzhi Sun[6,8], Qianwen Sun[1,3,*], Wei Xiong[1,2,*]

[1]School of Life Sciences, Tsinghua University, Beijing 100084, China

[2]IDG/McGovern Institute for Brain Research at Tsinghua University, Tsinghua University, Beijing 100084, China

[3]Tsinghua-Peking Joint Center for Life Sciences, Tsinghua University, Beijing 100084, China

[4]Department of Biomedical Engineering, Southern University of Science and Technology,1088 Xueyuan Road, Shenzhen, Guangdong 518055, China

[5]School of Life Sciences, Shandong University, 72 Binhai Road, Qingdao, Shandong 266237, China

[6]Chinese Institute for Brain Research, Beijing 102206, China

[7]Academy for Advanced Interdisciplinary Studies (AAIS), Peking University, Beijing 100871, China

[8]School of Basic Medical Sciences, Capital Medical University, Beijing 100069, China

[9]These authors contributed equally

[*]Corresponding Author

Wei Xiong, Ph.D.

School of Life Sciences

IDG/McGovern Institute for Brain Research at Tsinghua University

Tsinghua University

1 Qinghuayuan

Beijing 100084, China

Office: +86-10-62792464

Email: wei_xiong@tsinghua.edu.cn

Abstract

Frameshift mutation caused by small insertions/deletions (indels) often generate truncated and non-functional proteins, which underlies 22% inherited Mendelian disorders in humans. However, there is no efficient *in vivo* gene therapy strategies available to date, especially in postmitotic systems. Here, we leveraged the non-homologous end joining (NHEJ) mediated non-random editing profiles to compensate the frameshift mutation in a USH1F mouse model – *av3j*. After treatment by the selected gRNA, about 50% editing products showed reading-frame restoration, and more than 70% targeted hair cells recovered mechanotransduction. *In vivo* treatment ameliorated the hearing and balance symptoms in homozygous mutant mice. Furthermore, a scale-up analysis of 114 gRNAs targeting 40 frameshift deafness mutations reveals that 65% loci have at least one gRNA with predicted therapeutic potential. Together, our study demonstrates that the NHEJ-mediated frame restoration is a simple and highly efficient therapeutic strategy for small-indel induced frameshift mutations.

Main

The CRISPR/Cas9 based genome-editing techniques enable engineering pathogenic DNA variants, which has drawn significant attention on the

53 application for gene therapy in live animals[1,2]. The base-editing techniques

54 achieve correction of substitution mutations[3-5]. Homology-dependent strategies

55 can precisely correct mutations according to the given templates[6,7]. And

56 homology-independent editing strategies can introduce large insertion in

57 targeted region, thus leading to ameliorate disorders caused by large deletions[8].

58 However, specific and efficient therapeutic strategies for frameshift mutations

59 are still lacking. Following CRISPR/Cas9 cleavage, the induced DNA double

60 strand breaks (DSBs) are repaired by two major endogenous DNA repair

61 pathways, precise homology-directed repair (HDR) and error-prone non-

62 homologous end-joining pathway (NHEJ)[2]. Although the HDR pathway can

63 restore any mutations based on the given donor templates, its application is

64 largely limited due to low recombination efficiency and is almost absent in non-

65 dividing, terminally differentiated cells/organs[2]. While NHEJ is the major repair

66 mechanism but introduces stochastic indels, thus it has been widely applied in

67 reading frame disruptions. However, emerging evidence in dividing cells has

68 shown that the editing profiles through end-joining pathways are non-random

69 and mainly gRNA-sequence dependent[9-14]. Furthermore, gRNAs containing

70 dominant indels could be predicted by machine learning models[10,12,13], which

71 can compensate the pathogenic frameshift mutations, as exhibited in patient-

72 derived fibroblasts[12,15].

73 Here we adopted this NHEJ-mediated frame-restoration strategy and evaluated

74 its therapeutic potential *in vivo* within the context of hearing disorders. About

3

75 300 million people suffer from hearing loss worldwide, and 50% prelingual

76 hearing loss are caused by genetic mutations[16]. Among them, Usher Syndrome

77 is one of the most devastating diseases, which affect not only hearing, but also

78 vision and balance function[17]. However, there is no pharmacological treatment

79 available to date, especially for those types involving mutations in large proteins

80 (*USH1B*, MYO7A, 254 KD; *USH1D*, CDH23, 370 KD; *USH1F*, PCDH15, 216

81 KD; *USH2C*, VLGR1, 693 KD)[17]. In order to explore the frameshift correction

82 ability of this strategy for huge protein in postmitotic system, we recruited an

83 autosomal recessive USH1F mouse model – *av3j*, in which a spontaneous A

84 insertion causes frameshift in the 7.9 kb *Pcdh15* transcript and results in

85 truncated PCDH15 protein lacking transmembrane and intracellular domains[18]

86 (Fig. 1a). PCDH15 is one of the two components forming the tip link that gates

87 the mechanotransduction channels in inner-ear hair cells[19], including cochlear

88 outer hair cells (OHCs), inner hair cells (IHCs) and vestibular hair cells (VHCs).

89 The *av3j* mutant hair cells cannot detect mechanical force thus the homozygous

90 mice show profound congenital deafness and severe circling behavior.

91 By gRNA screening in cochlear explants, we identified one gRNA with half of

92 its profiles could compensate the 1-bp insertion in *av3j* mice. After genome

93 editing, the PCDH15 protein expression and localization were restored, and

94 nearly 3/4 targeted hair cells recovered mechanotransduction. Early postnatal

95 delivery of the gRNA-containing virus in scala media successfully ameliorate

96 auditory and vestibular symptoms of *av3j* homozygous mice. A scale-up gRNA

97   screening on postmitotic cochlear tissues revealed that this frame-restoration

98   strategy is suitable for more than 60% of the tested frameshift deafness sites.

99   Our results demonstrate that the NHEJ-mediated frame restoration is a simple

100   and highly efficient approach to correct small-indel induced frameshift

101   mutations, which opens up new perspectives for gene therapy strategy

102   targeting frameshift mutations, especially in postmitotic systems.

103

104   **Result**

105

106   **Design and characterization of gRNAs for frameshift restoration *ex vivo*.**

107   By searching the NGG PAM sequence proximal to the inserted A, four gRNAs

108   targeting *av3j* mutation were designed (Fig. 1b). The gRNAs with 17

109   nucleotides were used for higher editing specificity[20] . In order to interrogate the

110   genome editing outcomes in inner-ear cells, we established an *ex vivo* gRNA

111   screening system which combined cochlea culture, injectoporation[21], FACS,

112   and amplicon sequencing (Supplementary Fig. 1a). All designed gRNAs show

113   unique editing profiles, in which m-*3j*-gRNA1, wm-*3j*-gRNA9, and m-*3j*-gRNA21

114   preferred one or two dominant indel sizes while m-*3j*-gRNA24 had multiple

115   infrequent outcomes (Fig. 1c). Distinct profiles can be found between the

116   gRNAs with even 1-bp shift (m-*3j*-gRNA1, m-*3j*-gRNA21, and m-*3j*-gRNA24).

117   Considering *av3j* is a 1-bp insertion, we selected m-*3j*-gRNA1 that exhibits the

5

118   highest percentage of 1-bp deletion (D1) (red bars, Fig. 1c).

119   Next, we tested whether m-*3j*-gRNA1 could mediate functional restoration in

120   mutant *av3j/av3j* hair cells. Take advantage of our tissue injectoporation system,

121   we electroporated m-*3j*-gRNA1 and wildtype spCas9 (PX330-m-*3j*-gRNA1) in

122   postnatal day 3 *av3j/av3j* cochleae and cultured for 2 days *in vitro* (P3+2DIV).

123   PCDH15 puncta was specifically detected in some electroporated *av3j/av3j*

124   OHCs, at their hair bundle tips, but not in the surrounding unelectroporated hair

125   cells (Fig. 1d). GCaMP-based Ca^{2+} imaging was further applied to assess the

126   mechanotransduction recovery of electroporated *av3j/av3j* hair cells.

127   Surprisingly, among the 97 tested cochlear hair cells, including 81 OHCs (Fig.

128   1e,f) and 16 IHCs (Supplementary Fig. 1c), 72 restored responses to the

129   mechanical stimulation (74.2%, Fig. 1g), which was much higher than the 40.9%

130   D1 events showed in editing profiles (Fig. 1c), indicating that other frame-

131   restored products might be functional too.

132

133   **Function evaluation of the top frame-restored editing products for m-*3j*-**

134   **gRNA1***.*

135   To investigate the function of other frame-restored editing products, we further

136   analyzed the editing products of m-*3j*-gRNA1. There are mainly three frame-

137   restored types (refers to products with the same indel sizes): D1, 4-bp deletion

138   (D4) and 2-bp insertion (I2), and each frame-restored types contain 1-2 top

139   products (Supplementary Fig. 1d). We constructed the top editing products of

140   the three frame-restored types: PCDH15-E1373R (D1-top1), PCDH15-

141   E1373del (D4-top1) and PCDH15-E1373RK (I2-top1) (Supplementary Fig. 1e),

142   and further examined the functional recovery by electroporation and Ca^{2+}

143   imaging on *av3j/av3j* hair cells (Supplementary Fig. 1f,g). All frame-restored

144   constructs rescued the mechanosensitivity of electroporated *av3j/av3j* hair cells,

145   though the Ca^{2+} responses were smaller in PCDH15-E1373RK (I2-top1)

146   comparing to the wildtype PCDH15 control (Supplementary Fig. 1e-g). These

147   results show that almost all top frame-restored editing products of m-*3j*-gRNA1

148   can mediate functional rescue of *av3j/av3j* hair cells, though containing 1-2

149   amino acid alterations compared with WT protein sequences. All the frame-

150   restored products (3n-1) occupied 48.7% of total indels in m-*3j*-gRNA1 (Fig. 1h).

151   For mammalian cells are diploid and *av3j* heterozygous hair cells are fully

152   functional, so the function restoration rate of targeted hair cells would be

153   48.7%*48.7%+2*48.7%*(1-48.7%)=73.7%, which is consistent with the 74.2%

154   Ca^{2+} response recovery rate in the electroporated hair cells. These results

155   reveal that our frame-restoration strategy enables highly efficient reading-frame

156   correction and function restoration in postmitotic cells.

157

158   ***In vivo* editing profiles of m-*3j*-gRNA1 by virus delivery.**

159   To achieve the genome editing *in vivo*, we packed the U6-gRNA scaffold into

160 the AAV2/9 capsid, with a mCherry expression cassette included to indicate

161 virus transfection. Firstly, a preliminary transfection was applied to WT mice by

162 scala media injection at P0-P2. The mCherry expression was observed in 100%

163 IHCs in all observed cochleae at 14 day-post-delivery (PVD), and the

164 transfection rates in OHCs and VHCs was 70% and 60%, respectively

165 (Supplementary Fig. 2).

166 Then we assessed the *in vivo* genome editing profiles of m-*3j*-gRNA1 in

167 *av3j/av3j* mice with *Cas9* knockin background[22] (*av3j/av3j;Cas9+*). The

168 cochlear and vestibular tissues were harvested at 2, 4, 8, 12, and 16 weeks

169 PVD (Supplementary Fig. 3a-d). The averaged editing efficiencies were 60%

170 for cochlear tissues and 70% for vestibular organs, which reached a plateau as

171 early as 4 weeks, with the major editing events carried out within 2 weeks (Fig.

172 2b). When comparing the detailed editing profiles in cochleae and vestibules *in*

173 *vivo* with that from cochleae *ex vivo*, we found that D1 and I1 were dominant at

174 all tested conditions. Although the exact frequencies vary (Fig. 2c-e), the

175 dominant frame-restored products are exactly the same, as manifested by the

176 indel positions and inserted bases (Fig. 2f-h). Besides, the editing outcomes

177 are more similar in profiles from cochleae (*in vivo* and *ex vivo*) compared to

178 those from vestibular organs, indicating a system-specific bias in editing profiles.

179 As previous study showed a recut of small indel products to larger deletions[9],

180 we studied the editing profiles along time, and found that the outcomes of

8

181 virally-delivered m-*3j*-gRNA1 were stable at all tested time points

182 (Supplementary Fig. 3e,f). We also tested the off-target effects for this long-

183 term AAV-mediated expression by amplicon sequencing of predicted off-target

184 sites (see Methods). 2 out of 16 selected off-target sites show detected editing

185 with averaged indel frequencies at 0.7% and 0.3% (Supplementary Fig. 3g,h).

186 These results demonstrate that our *ex vivo* screening and evaluation indeed

187 help assess the therapeutic potential of gRNAs for the frame-restoration gene

188 therapy *in vivo*.

189

190 **NHEJ-mediated frame restoration recovers mechanotransduction of *av3j***

191 **hair cells *in vivo*.**

192 We initially examined the PCDH15 protein expression and localization in

193 treated mice after virally delivering m-*3j*-gRNA1 at P0-2. The PCDH15 protein

194 expression is recovered after the treatment, as PCDH15 puncta was observed

195 in the hair bundle tips of the transfected *av3j/av3j;Cas9+* OHCs at 5 days PVD

196 (Fig. 3a).

197 To investigate the recovery of mechanotransduction, fluid-jet evoked currents

198 were monitored by whole-cell patch-clamp recording on auditory hair cells at 10

199 days PVD (Fig. 3b). Among these transfected hair cells, 14 out of 20 OHCs and

200 18 out of 19 IHCs restored mechanotransduction currents (Fig. 3c,d), which is

201 consistent with the high recovery efficiency observed *ex vivo*.

9

202   To assess the *in vivo* functional rescue ratio in targeted auditory hair cells, we

203   used styryl FM5-95 dye to label the function-restored hair cells. Styryl FM dye

204   has been reported entering to hair cells through mechanotransduction channels,

205   thus it is used as an indicator for channel opening[23]. In total of 929 counted

206   transfected OHCs, 78.3% recovered dye uptake (Supplementary Fig. 4a,b). As

207   previous study has shown a gradual hair cell loss in *av3j* homozygous mice[24],

208   to evaluate whether our treatment could reverse this symptom, we next

209   quantified the hair-cell survival in injected cochleae. After treatment, hair-cell

210   survival was improved in the apical turn, while the cell death in the middle and

211   basal turn was not significantly reversed (Supplementary Fig. 4c-g).

212

213   **NHEJ-mediated frame restoration recovers auditory function of *av3j* mice**

214   ***in vivo*.**

215   To evaluate whether the auditory function of injected *av3j/av3j;Cas9*+ mice was

216   rescued, we recorded the auditory brainstem response (ABR) at 4-5 week PVD.

217   15 out of 33 injected mice showed obvious ABR responses, compared to totally

218   no signals in the uninjected animals (Fig. 3e-d). And the maximum click ABR

219   threshold improvement was up to 20 dB, with 3 best mice harbored pure-tone

220   ABR threshold at 80 dB SPL for 11.3 kHz. However, the lack rescue of the other

221   18 injected mice was unclear, may have been due to lower virus transfection

222   rates.

223   In order to evaluate the recovery of whole auditory circuits, acoustic startle

224   responses were tested by random white noise stimulation of multiple sound

225   intensities. Obvious startle responses could be recorded in some injected

226   mutant mice upon large stimuli. 17 injected *av3j/av3j;Cas9+* mice were tested

227   in acoustic startle test prior to ABR recording, in which 11 had both startle and

228   ABR recovery, 4 with ABR recovery only, and the rest 2 with no restoration in

229   both assays (Fig. 3g). These data demonstrate that highly efficient, postnatal

230   recovery of hair-cell mechanotransduction could reverse the totally abolished

231   hearing loss in *av3j* mice.

232

233   **NHEJ-mediated frame restoration recovers vestibular function of *av3j***

234   **mice *in vivo*.**

235   As *av3j* mice also has severe balance problem due to totally abolished

236   mechanotransduction in VHCs, we further evaluated the functional rescue in

237   vestibular system. In the transfected *av3j/av3j;Cas9+* VHCs, protein expression

238   of PCDH15 was also detected at 10 days PVD (Fig. 4a). In 11 transfected VHCs,

239   7 restored mechanotransduction currents (10 days PVD, Fig. 4b-c).

240   To evaluate the overall vestibular function in injected *av3j/av3j;Cas9+* mice,

241   we recorded the vestibulo-ocular reflex (VOR), in which the vestibular system

242   detects head motions and triggers opposite eye movements to help vision

243   stabilization. The injected mutant mice showed VOR response recovery close

11

244 to wild-type levels at all tested rotation frequencies, in contrast to the totally

245 absent VOR in the uninjected mice (Fig. 4d-e). Then we performed open field

246 and rotarod test to examine the restoration of balance behavior. The circling

247 frequencies were also reduced in some injected *av3j/av3j;Cas9+* mice, as 7 out

248 of 21 animals almost stopped circling (Fig. 4f-g). In rotarod test, all injected

249 *av3j/av3j;Cas9+* animals stayed longer on the rotating rod comparing to the

250 uninjected mutants (Fig. 4h). And 6 injected mice could still stand on the rod

251 when the tests had finished at 300 s just like the majority of WT animals,

252 indicating almost full recovery of the balance function.

253

254 **Therapeutic gRNA screen for other frameshift deafness mutations**.

255 After the successful therapeutic application of this frame-restoration strategy on

256 *av3j* mice, we further explored whether it can be extended to target other similar

257 disease mutations with our *ex vivo* gRNA screening system (Supplementary

258 Fig.1a). A total of 114 gRNAs were designed to target 40 human pathogenic

259 deafness mutations that are caused by 1-bp indels, and only the highly similar

260 sequences between humans and mice were selected (Supplementary Table

261 1,2). During the gRNA screening for *av3j* site, we found that the indel

262 distributions and indel positions were very similar between gRNA pairs targeting

263 the same genomic sites in *av3j* genome and WT genome, which share the

264 same PAM positions and differ only in the 1-bp A insertion (Supplementary Fig.

265   5a-f). We next used the published genome editing prediction models, inDelphi[12]

266   and FORECasT[10], to predict the editing profiles of 114 gRNA pairs targeting

267   mutant genomes and WT genomes. Most gRNA pairs showed high correlations

268   of their editing profiles (median Pearson *r*: inDelphi, 0.84; FORECasT, 0.90,

269   Supplementary Fig. 5 g-j). All these indicate that the mutant and WT gRNA pairs

270   share similar editing profiles. As the *ex vivo* results resemble the *in vivo* editing

271   profiles (Fig. 2), electroporation on WT cochlear tissues was applied to

272   investigate the editing profiles of the designed gRNAs.

273   For frame-restoration gRNA selection, multiple factors were considered in

274   defining the therapeutic potential (Fig. 5a). Firstly, only gRNAs that mediate

275   successful genome editing have the possibility of frameshift correction (editing

276   efficiency). And fraction of frame restoration provides a baseline for function-

277   rescue evaluation. For those sites tolerant for small amino acid changes, this

278   factor may directly reflect the function-rescue fraction, thus enabling a quick

279   evaluation of available gRNAs. Then the function of frame-restored products,

280   which lays the foundation of final therapeutic outcome, is the key point in gRNA

281   evaluation.

282   All designed gRNA showed different editing efficiencies (Fig. 5b) and fraction

283   of predicted frame restoration (Fig. 5c). As for the function of the frame-restored

284   editing products, we quantified the predicted amino acid changes (Fig. 5d), and

285   assumed that with fewer amino acid changes, the products have higher

286 possibilities to achieve a final functional rescue. Besides the absolute altered

287 numbers, the functional importance of affected amino acids is also relevant for

288 functional evaluation of the editing products. So we did conservation analysis

289 of each amino acid position near the mutant sites[25]. In order to link the

290 conservation status and amino acid change number to the final protein function,

291 we selected 24 editing products targeting 6 deafness sites, and validated their

292 protein functions in either HEK293T cells or electroporated cochlear hair cells

293 (Supplementary Fig. 6). In general, with lower conservation of altered amino

294 acid, there is a higher possibility of protein function preservation. Some

295 unconserved regions are tolerant for as many as 3 amino acid alterations,

296 including both deletions and substitutions. And in many cases, deletions were

297 more deleterious than substitutions (Supplementary Fig. 6). We incorporated

298 all our observations into one functional prediction algorithm to help briefly

299 evaluate the fraction of function-restored editing products in each gRNA (for

300 details, see Methods).

301

302 **Radar plot assists evaluation and selection of therapeutic gRNAs for**

303 **frameshift mutations**.

304 Finally, we integrated all these parameters into one radar plot to facilitate the

305 therapeutic gRNA evaluation and selection (Fig. 6). The radar plot has 5

306 axis: *%Indel*; *%Frame-restoration*; *%Predicted aa changes* ≤3, showing

14

307   percentage of editing products with equal or less than 3 amino acid changes

308   compared with WT protein sequences; *%Predicted functional rescue*, the

309   fraction of products with a predicted functional rescue; *Specificity*, a specificity

310   score, which based on sequence homology across mouse genome, was

311   calculated by published algorithms[26] (for details, see Methods). From radar plot,

312   w-*TMC1*-229dA-g1 was predicted as the best for *TMC1* c.229delA mutant site

313   (Fig. 6a,d,g). For *PCDH15*-16dT, which locates in highly variable region, both

314   two designed gRNAs could mediate high fractions of predicted function-rescue

315   products (Fig. 6b,e,h). And for USH1C c.369delA mutation, w-*USH1C*-369dA-

316   g1 would have the best performance (Fig. 6c,f,i). Note that, cleavage sites of

317   w-*USH1C*-369dA-g3 and w-*USH1C*-369dA-g4 only separate 1-bp away, and

318   they generate many identical editing products. Although w-*USH1C*-369dA-g3

319   has more frame-restored products and similar protein alteration spectrum

320   compared with w-*USH1C*-369dA-g4, it contains the lowest functional rescue

321   products, for w-*USH1C*-369dA-g3 preferred more amino acid deletions instead

322   of substitutions compared with w-*USH1C*-369dA-g4 (Supplementary Fig. 6c,d).

323

324   **Discussion**

325   Here we present an *in vivo* genome editing strategy exhibiting unprecedented

326   correction efficiency of frameshift mutations in postmitotic system, which is

327   based on the highly biased, NHEJ-mediated editing outcome. In our *av3j* case,

15

328   nearly 75% genome edited hair cells restore mechanotransduction, and this

329   highly effective cell-level recovery further ameliorate auditory and vestibular

330   symptoms in this USH1F animal model. As NHEJ is the major DSB repair

331   pathway in almost all cell types, including both dividing and non-dividing cells[27],

332   in theory, this strategy enables efficient frame restoration in virtually any

333   cells/organs. Besides, no editing template is required for this strategy, which is

334   the necessity for HDR-mediated precise editing, thus it largely eases the

335   strategy design and delivery procedure.

336   Our gRNA screening data reveal that gRNAs shifted in only 1-bp may exhibit

337   totally different editing profiles with distinct dominant indels and indel size

338   distributions, e.g. m-*3j*-gRNA1, m-*3j*-gRNA21 and m-*3j*-gRNA24 (Fig. 1b,c).

339   Though some of these gRNAs may generate identical editing products, the final

340   function-rescue fractions vary a lot for the different product frequencies, e.g. w-

341   *USH1C*-369dA-g3 and w-*USH1C*-369dA-g4 (Fig. 6c,f,i). And in many cases,

342   more than one gRNA are available for one frameshift mutation. These results

343   demonstrate that the NHEJ-mediated frame-restoration strategy also enables

344   highly flexible choice for therapeutic gRNAs.

345   In the past decade, great achievement has been obtained on gene therapy of

346   inherited deafness. Gene replacement is the most common and successful type

347   of genetic manipulation in this field[28-33], which however is limited by the loading

348   capacity of delivery vectors, e.g. 4.7 kb for AAV, rendering gene therapy for

16

349   large proteins almost impossible. Recent progress on genome-editing-based *in*

350   *vivo* deafness gene therapy showed significant hearing improvement on

351   progressive hearing loss models, which harbor missense mutations on *TMC1*

352   (cDNA 2.3kb), using either reading-frame disruption of dominant-negative

353   allele[34,35] or base editing[36]. Here, we provide the first study of large protein

354   frame-restoration in a congenital profound deafness model, and also prove the

355   possibility of USH1F amelioration by postnatal genetic manipulations.

356   Before our study, there are several studies also leveraged the non-random

357   CRISPR cleavage and repairing patterns to correct pathogenic mutations[12,15].

358   MMEJ-mediated larger deletions were used to rescue pathogenic

359   microduplication to wildtype sequences, which are relatively controllable for one

360   could search for the microhomology arms and precisely predict the editing

361   outcomes. Here, we take advantage of the NHEJ-mediated insertions and

362   deletions, which are the dominant components of most editing outcomes, to

363   compensate the small indels in frameshift mutations while leaving 1-2 amino

364   acid alterations in the frame-restored products. Our data reveal that for some

365   less important regions, imperfect correction could also mediate a significant

366   phenotypic restoration.

367   During our explorations in *av3j* treatment, we find that for recessive mutations

368   in diploid mammalian cells, only one functional allele is enough to achieve a

369   cell-level functional rescue. Thus, gRNAs with 30% functional rescued products

370   could provide about 50% function restoration cells containing diploid genomes.

371   In our 114 gRNA screening, 55 of them could achieve this criterion, covering

372   65% (26/40) selected deafness mutations. If the percentage of function-

373   restored cells are above the 'minimal requirement' for a system to conduct

374   physiological function, a phenotypic restoration could be achieved. Once a

375   gRNA could provide enough function-restored cell fraction for the targeted

376   system, it deserves to try for *in vivo* applications.

377   Though we got some auditory function restoration in the USH1F mice, yet the

378   rescue effect is still limited. Combining the nearly 75% functional recovery rates

379   (Fig. 3b-d and Supplementary Fig. 4a,b) with the 100% and 70% transfection

380   ratios in IHCs and OHCs (Supplementary Fig. 2f), around 75% IHCs and 53%

381   OHCs could be recovered in the injected mice, thus the majority of hair cells

382   were rescued by our treatment. However, unrecovered and disorganized hair

383   bundles were observed along the entire cochleae in all tested, virus-delivered

384   mice, which may also underlie the smaller mechanotransduction currents in

385   targeted OHCs (Fig. 3c). And the irreversible cell death in middle and basal turn

386   may further indicate that PCDH15 is not only important for hair-bundle

387   development and organization, but also relevant for hair-cell maintenance and

388   survival. Considering that the PCDH15 starts expression as early as embryonic

389   day 12[37], further study is needed to map the best therapeutic window for this

390   protein.

391 Here we demonstrate the first *in vivo* gene therapy for frameshift mutation in a

392 postmitotic system, and provide a practical guide for frame-restoration gRNA

393 evaluation and selection. We anticipate that, with further improvement in profile

394 prediction of mutant genomes and functional evaluation on edited products, this

395 NHEJ-mediated frame-restoration strategy holds great promise for clinical

396 treatment of small indels induced frameshift mutations, which consists 22% of

397 the inherited Mendelian disorders in humans[38].

398

399 **Methods**

400 **Animals**

401 All animal experiments were performed in compliance with the guidelines

402 provided by the Institutional Animal Care and Use Committee (IACUC) at

403 Tsinghua University. The mice were maintained in the Animal Research Facility

404 in campus, which has been accredited by the Association for Assessment and

405 Accreditation of Laboratory Animal Care International (AAALAC). Both

406 *av3j/av3j* mice[18] (C57BL/6J-*Pcdh15*[av-3J]/J, JAX:002072) and *v2j/v2j* mice[39]

407 (C57BL/6J-*Cdh23*[v-2J]/J, JAX:002552) were gifts from Dr. Ulrich Müller. The

408 *av3j/av3j;Cas9+* mice were achieved by crossing *av3j/av3j* mice with the Cas9

409 knockin mice[22] (Gt(ROSA)26Sor[tm1.1(CAG-Cas9*-EGFP)Fezh], JAX:024858, Bar Harbor,

410 ME). The mice were housed in a temperature-controlled room with 12-hr

411 light/dark cycle and have free access to water and food. Both female and male

412   mice were used.

413

414   **Design of gRNAs and plasmid construction**

415   All gRNAs were constructed with the PX330 backbone (42230, Addgene). The

416   primers used for plasmid construction were designed by CCtop

417   (CRISPR/Cas9 target online predictor, https://crispr.cos.uni-heidelberg.de)

418   with default parameters, except for setting the gRNA length to 17 nt. The

419   plasmids were constructed as previously reported[40]. Briefly, the oligos were

420   phosphorylated by T4 Polynucleotide Kinase (M0201S, NEB) at 37°C for 30

421   min, then annealed by temperature ramping from 95°C to 25°C in a

422   thermocycler. The PX330 backbone was digested with BbsI (R0539S, NEB),

423   and ligated with the oligos by T4 ligase (15224017, Invitrogen). The plasmids

424   were extracted by MaxPure Plasmid HC kit (P1231, Magen, China) for

425   following procedures including cell-line transfection and tissue electroporation.

426

427   **Cell/tissue culture and transfection**

428   The N2a cell line was a gift from Dr. Yichang Jia (Tsinghua University), and was

429   maintained in normal DMEM (C11965500BT, Thermo Fisher) containing 15%

430   fetal bovine serum (AB-FBS-0500s, ABW) and 100 U/ml penicillin-streptomycin

431   (15140148, Thermo Fisher). The N2a cells were seeded in 48-well plate in ~70%

432 confluence at 24 hr before the transfection. The plasmids were transfected with

433 Lipofectamine 2000 (11668019, Thermo Fisher) following manufacturer's

434 instructions. Normally, N1-EGFP was co-transfected to guarantee successful

435 transfection.

436 Cochlear culture and injectoporation were as previously described[21]. In this

437 study, the organ of Corti was dissected out from mouse pups and was attached

438 on the inner side of a 35-mm culture dish lid cultured with 2ml DMEM/F12

439 medium (21041-025, Thermo Fisher) with ampicillin (1.5 μg/ml, GG101,

440 TransGen Biotech) addition. For electroporation, plasmids (1 μg/μl in 1x HBSS)

441 were injected into gaps between hair cells via a glass electrode with an open

442 tip of 2 μm diameter. A series of 3 electrical pulses (80-V amplitude, 20-ms

443 duration, 1-s interval) were immediately applied by an electroporator (BTX

444 ECM830, Harvard Apparatus). After electroporation, the tissues were cultured

445 in a humid incubator (37°C, 5% CO_2).

446

447 **Immunofluorescence**

448 For PCDH15 immunostaining, cultured or fresh dissected cochlear tissues were

449 pre-treated with phosphate buffered saline (PBS, cc0005, Leagene; calcium

450 free) adding 5 mM EGTA (E3889, Sigma-Aldrich) for 10 min at room

451 temperature (RT), then fixed in 4% paraformaldehyde (PFA, DF0135, Leagene)

452 for 10 min at RT. Then washed for 5 min x 3 times and blocked in 1% BSA

21

453 (A3059, Sigma-Aldrich) (w/v) for 1 hour at RT before incubating with antibodies.

454 Primary antibody: rabbit anti-PCDH15 (PB811, 1:400 dilution, a gift kindly

455 provided by Dr. Ulrich Müller), incubate at 4°C for 16 hours followed by 15 min

456 x 3 times wash in PBS. Secondary antibodies: goat anti-rabbit (A-21245, Alexa

457 647 conjugated, Thermo Fisher, 1:500) with either Alexa Fluor 488 (A12379,

458 Thermo Fisher, 1:1000) or Alexa Fluor 568 Phalloidin (A12380, Thermo Fisher,

459 1:1000), incubate at RT for 2 hours followed by 15 min x 3 times wash in PBS.

460 All antibodies were diluted in PBS with 5 mM EGTA by v/v. The tissues were

461 finally mounted with ProLong Gold Antifade Mountant (P36930, Thermo Fisher).

462 The images were acquired using a deconvolution microscope (DeltaVision,

463 Applied Precision) equipped with a 100x oil-immersed objective and

464 deconvolved using the Huygens deconvolution software (version 18.10, SVI).

465 For virus transfection and hair cell survival quantification, animals were

466 sacrificed and harvested the inner ear tissues. Then fixed in 4% PFA for 30min

467 at RT, washed in PBS by 7 min x 3 times. Dissected the basilar membrane and

468 blocked in 1% FBS for 1 hour at RT before incubating with antibodies. Primary

469 antibody: rabbit anti-Myo7a (25-6790, Proteus Biosciences Inc, 1:1000)

470 incubate at 4°C overnight and followed by 15 min x 3 times wash in PBS.

471 Secondary antibodies: goat anti-rabbit Alexa 647 conjugated at 1:2000 with

472 Alexa Fluor 488 Phalloidin (1:1000). The tissues were finally mounted with

473 ProLong Gold Antifade Mountant. The images were captured using Andor

474 Dragonfly spinning disk confocal microscopy by the 40x oil-immersed objective.

475 The spot and filament function of Imaris Software v9.3.1 (Oxford Instrument)

476 were used for cell number quantification. For virus transfection quantification,

477 gamma values were set to 3, in order to show clear labeling in the weak viral

478 expression cells.

479 For functional tests on HEK293T cells, cells were transfected with EGFP-

480 fused harmonin with or without mutations. Harvest 24hr-post-transfection,

481 followed by 3 wash in PBS, and fixed in 4% paraformaldehyde (PFA, DF0135,

482 Leagene) for 15 min at RT. Then washed 3 times in PBS. And stained with

483 Phalloidin- Alexa Fluor 568 (A12380, Thermo Fisher, 1:1000) at 4°C overnight.

484 Wash 3 times in PBS. Images acquired by Zeiss LSM780 confocal microscope

485 using 100X (NA 1.4) oil-immersion objective. Maximum projections of z-stacks

486 were handled using Zeiss Black software.

487

488 **Tissue analysis**

489 ***Cochlea calcium imaging***

490 The genetically encoded Ca2+ indicator GCaMP6m-X[41] was co-transfected in

491 cochlear hair cells. For calcium imaging, the tissues were bathed in fresh

492 external solution (in mM): 144 NaCl, 5.8 KCl, 2.5 $CaCl_2$, 0.9 $MgCl_2$, 10 HEPES,

493 5.6 D-Glucose, PH7.4. A series of three fluid-jet stimuli (20 psi, 0.1 s, 0.3 s and

494 0.5 s) were applied by a glass capillary with an open tip of 5 μm diameter at 40-

495 s interval. Images were acquired with an upright microscope with a 60x water-

496   immersed objective (Olympus BX51WI) at 2-s sampling rate.

497

498   ***Whole-cell electrophysiology of hair cells***

499   At assigned ages, the mice were sacrificed and their apical part of basilar

500   membrane or whole saccules were taken out and transferred into dissection

501   solution, which contains (in mM): 5 KCl, 140 NaCl, 1 $MgCl_2$, 0.5 $MgSO_4$, 0.1

502    $CaCl_2$, 10 HEPES, 3.4 L-Glutamine, 10 D-Glucose, pH 7.2. The tectorial

503   membrane or otolith was removed with fine forceps, then the organ of Corti or

504   sacculus was transferred into a recording dish with recording solution, which

505   contains (in mM): 145 NaCl, 0.7 NaH_2PO_4, 5 KCl, 1.3 $CaCl_2$, 0.9 $MgCl_2$, 10

506   HEPES, 5.6 D-Glucose, pH 7.4. Then mCherry expressed OHCs or VHCs were

507   whole-cell recorded and membrane currents were measured by an

508   electrophysiology amplifier (EPC-10 USB, HEKA, Germany) at sampling rate

509   of 20 kHz. The cells were held at –70 mV and the hair bundle was stimulated

510   by a fluid jet. For OHCs, 40-Hz sinusoid stimulation in 60 ms was performed.

511   For VHCs, a 500-ms square wave was used in order to obtain large enough

512   stimulation.

513

514   ***FM5-95 loading and imaging***

515   Wild type C57B6J animals and *av3j/av3j;Cas9+* animals with or without virus

516 injection were sacrificed at P7-P10. Basilar membranes were dissected in 1 X

517 HBSS and bathed in 6uM ice-cold FM5-95 (T23360, Thermo Fisher, dissolved

518 in 1 X HBSS) for 30s, then followed by 4-5 washes in clean HBSS. Tissues

519 were attached to glass bottom dish upside down by prolong-antifade solution.

520 Images were obtained using Zeiss LSM880 confocal microscope equipped with

521 standard laser lines (405 , 514 , 561 ,633 nm) using 40 X (NA 1.2) water-

522 immersion objective. Maximum projections of z-stacks were handled using

523 Zeiss Black software. FM5-95 was excited by 514-nm laser and monitored in

524 the region between 680-742nm, an emission wavelength to distinguish from

525 GFP signal (Cas9 KI) and mCherry signal from virus.

526

527 **Genome editing analysis**

528 ***Tissue digestion and FACS***

529 Electroporated or AAV-transfected auditory tissues (containing basilar

530 membrane, spiral ligament, and stria vascularis) and vestibular tissues (include

531 utricles, saccules and semicircular canals) were dissected in ice-cold HBSS

532 (C14175500CP, Thermo Fisher) quickly and then incubated in HBSS with 1

533 mg/ml collagenase I (C0130-1g, Sigma-Aldrich) and 0.05% trypsin-EDTA

534 (25200056, Thermo Fisher) at 34°C for 10-15 min. The effect of enzymatic

535 dissociation was checked with an inverted microscope. Then equal volume of

536 10% FBS-containing DMEM/F-12 medium was added to stop the reaction. After

537   centrifuging at 1,000 g for 1min, the cells were washed with 10% FBS-

538   containing DMEM/F-12 and re-suspended. After passing through a 70-μm filter

539   to remove large debris, the isolated cells with fluorescence signals were sorted

540   and enriched directly into 0.2-μl PCR tubes by a FACS machine (BD Influx).

541   Noted that, in order to get enough cells for downstream deep sequencing, the

542   FACS gate was relatively loose to collect total cells containing red cells at 5-

543   20%.

544

545   ***Deep sequencing library construction and data analysis***

546   Genome DNA of transfected N2a cells or tissue cells were extracted by

547   QuickExtract™ DNA Extraction Solution 1.0 (QE09050, Lucigen, Middleton, WI)

548   following the manufacturer's instructions. For each targeting genome locus, an

549   amplicon of 100-300 bp was designed, with cleavage sites located about 50-

550   100bp away from amplicon boundaries. Firstly, the first run of PCR (PCR1) was

551   applied to amplify targeting DNA with primers containing part of the Ilumina

552   adaptors. And exonuclease I was added to the PCR1 products to clear all

553   remaining PCR1 primers. Then a second run of PCR was performed to add

554   unique barcodes and P5/P7 flow cell binding sites. All the PCR reactions were

555   carried out with Kapa HiFi 2 x mastermix (KK2601, Kapa Biosystems). PCR

556   products were then separated by 2% agarose gel, and only products with

557   desired sizes were cut and purified by Gel Purification kit (D2110, Magen,

26

558 China). After quantified by Qubit™ 1X dsDNA HS Assay Kit (Q33230, Thermo

559 Fisher) and verified by Agilent 2100 Bioanalyzer, samples were pooled together

560 and sequenced 2X150 on the Illumina HiSeq X-Ten platform. Sequencing reads

561 were demultiplexed according to the 8-nt index sequence and then individual

562 FASTQ files were analyzed by the batch version of CRISPResso2 v.2.0.32[42]

563 with the CRISPRessoPooled mode. The analysis parameters were set as: -w

564 12, -q 30, -s 0, --max_paired_end_reads_overlap 150, while others were used

565 as default. And all other analysis and quantification were based on the

566 "Alleles_frequency_table.txt" in the CRISPResso2 report with custom Python

567 scripts or Excel2016. Noted that, all our editing analysis exclude reads with only

568 substitution. The indel frequency were calculated as (all edited reads –

569 substitution only reads)/(all reads for the target locus).

570

571 ***Off-target prediction***

572 The mismatch off-targets were predicted by CCtop[43] (CRISPR/Cas9 target

573 online predictor, https://crispr.cos.uni-heidelberg.de). All the mismatched off

574 targets were ranked by number of mismatches, then the off-target loci were

575 chose with different alignment parameters. The off targets with DNA bulges

576 were predicted by Cas-OFFinder[44] (http://www.rgenome.net/cas-offinder/), set

577 the DNA bulge size to 1bp. Off-target loci with different bulge locations were

578 chosen. Noted that, all selected bulge loci also had 1 bp mismatch with the on-

579 target site. And all off-targets avoided repeating region.

580

Function prediction of editing product

582 We used "Alleles_frequency_table.txt" in the CRISPResso2 report as the input

583 files for the function prediction analysis. The "MODIFIED" reads were first

584 aligned with WT CDS sequences to obtain the CDS region. Then create the

585 predicted editing products in mutant genomes by manually adding the ±1-bp

586 mutations into the editing reads based on WT genomes using following rules:

587 for 1-bp deletion mutations, if the deletion positions were not edited, delete the

588 base at the deletion position, otherwise, delete the bases closest to the 3-bp

589 upstream the PAM sequences; for 1-bp insertion mutations, if the insertion

590 positions were not edited, insert the bases in the insertion sites, otherwise

591 inserted the mutant bases at positions that make the edited indels have closest

592 distances with the 3-bp upstream the PAM sequences. Only the predicted

593 products that were multiples of 3 would be translated into protein sequences

594 and continued function prediction.

595 Each amino acid position was assigned to the conservation score (rank

596 from 1 to 9, from the highly variable to highly conserved, corresponded to the 9

597 color codes in figures) calculated by ConSurf 2010[45] (http://consurf.tau.ac.il)

598 using parameters: multiple sequence alignment using MAFFT; homologues

599 collected from UNIREF90; homology search algorithm using HMMER (E-value

600 0.0001, No. of iteration 1); maximal %ID between sequences:95; minimal %ID

601 for homologs:35; using 150 sequences that sample the list of homologues;

602 method of calculation: Bayesian; model of substitution for proteins: best fit.

603 And the predicted product would be predicted as nonfunctional if it satisfy

604 any of following criteria:

605 1. Containing any stop codons;

606 2. For amino acid deletion: deleted highly conserved amino acids (conservation

607 score ≥7) and or deletion happen near highly conserved amino acids (one or

608 both neighboring amino acid score =9);

609 3. For amino acid insertion: insertion happen in between highly conserved

610 amino acids (both neighboring amino acid score ≥7);

611 4. Total amino acid changes ≥ 3, including substitutions, insertions and

612 deletions;

613 5. Substitution of highly conserved amino acids (conservation score ≥7), and

614 the amino acid switches did not exist during evolution;

615 6. Substitution of highly conserved amino acids (conservation score ≥7), and

616 the amino acid switches change the acid-base property of the amino acid

617 position.

618

619 ***Specificity prediction of gRNAs***

620 The gRNA specificity were calculated in Benchling

29

621 (https://www.benchling.com/), which enable scoring gRNA with 17-nt length. A

622 uniform formula, based on off-target mismatch and mismatch position[46], were

623 used to calculate a specificity score for each gRNA, thus enabled a comparison

624 of gRNA specificity even in different loci.

625

626 ***Radar plot drawing***

627 In the radar plot, the value of each axis was in linear distribution, with the max

628 value located in the outermost ring. The maximal values

629 of %Inframe, %Predicted aa change ≤ 3, %Predicted functional rescue were

630 set to 100%. And the center was set to 0%. The value of the outermost ring was

631 15% for %Indel and 45 for specificity.

632

633 **Animal treatment and analysis**

634 ***Surgery and virus injection***

635 All AAVs used in this study were customized from Vigene Bioscience, Jinan,

636 China. For anesthesia, P0-1 mice were put on ice and waited for 1-2 min. Then

637 dorsal incision was made, and the ear was approached to expose the bulla.

638 With a stereotaxic microscope, the scala media was visually located between

639 the round widow niche and the stapedial artery, then 600-nl virus solution (1.5

640 $\times 10^{14}$ vg/ml) was injected into scala media at a rate of 250 nl/min. Fast green

641 (F7258, Sigma-Aldrich) was added to visualize delivery effect, as successful

642 delivery to scala media came with a ribbon pattern. For each pup, both ears

643 were injected and all procedures were finished within 20 min.

644

Auditory brainstem response (ABR)

645

646 Mice were anesthetized by intraperitoneal injection of tribromoethanol (300

647 mg/kg). The recording electrode was inserted underneath the scalp right

648 between the two ears. The reference electrode and the ground electrode were

649 inserted subcutaneously at the pinna and the groin respectively. ABR data were

650 collected by an RZ6 workstation controlled by a BioSig software (Tucker-Davis

651 Technologies, Alachua, FL). Pure tone stimuli was applied at 4, 5.6, 8, 11.2, 16,

652 32 kHz. Maximum stimulus intensity was set to 90 dB SPL, with attenuation

653 decreasing from 110 dB to 10 dB SPL at 5-10dB steps.

654

Vestibulo-ocular reflex (VOR) and data analysis

655

656 The VOR recording and data analysis was conducted as previously reported[47].

657 Briefly, in a metal chamber, the mouse was immobilized by a clamp and

658 mounted on a mirror-camera-equipped turn table. Then the binocular eye

659 movements were evoked by ± 20° sinusoidal rotations at 0.25, 0.5, or 1 Hz

660 frequencies. For each animal, a 2-3 min video was recorded and traced by a

661 custom machine-learning-based scripts in matlab R2016a. The horizontal eye-

662 move degree was calculated as

663 $$\alpha = EH*180/pi*RP$$

664 Where α indicates horizontal eye-movement degree, EH indicates horizontal

665 eye-movement distance, and pi means the Constant of PI, and RP indicates

666 the axial length of eye-movement[48]. Six periods, whose peak frequency

667 coincided with stimulus frequency, were averaged to calculate the final eye

668 movement angles. The gain value was calculated as:

669 Gain = (Eye movement angle)/(Platform stimulation angle).

670

671 ***Open field test and data quantification***

672 4~8 week-old animals were used for all behavior tests. A 33 X 33 cm arena was

673 used with infrared illumination. Animals were placed on one side of the arena

674 and videotaped for 10 min. The arena was cleaned before changing to another

675 animal. The circling behaviors were quantified by a behavior analysis software

676 (The EthoVision XT version 11.5, Noldus Information Technology). Both

677 clockwise and anticlockwise circling were counted in analysis of circling

678 frequency. And the moving traces are tracked by custom MATLAB scripts.

679

680 ***Rotarod test***

32

681 Before test, animals were trained on a rotarod (47650, Ugo Basile) for 5 times

682 in 2 days, by which first two workouts used constant 10 r.p.m for XX s, and the

683 next three were the final 300-s test program that began at 10 r.p.m and then

684 increased to 30 r.p.m in 90 s. During test, each animal ran 5 times to count the

685 running time before it fell from the rotarod. After excluding the maximum and

686 minimum, the averaged running time was used for data presentation.

687

688 ***Acoustic startle response***

689 The acoustic startle responses were recorded by Xeye Startle Reflex system

690 (v1.2, Beijing MacroAmbition S&T Development). The animals were tested in a

691 sound shielded startle box and the startle responses were sensed by the

692 gravitational acceleration sensor fixed beneath an elevated platform. Mice were

693 placed in a smaller, squared, plastic chambers and anchored to the sensing

694 platform during recording. Experiment started with a 5 min 60dB background

695 white noise, and then followed by 32 trials of single noise pulse presented at

696 pseudorandom order at randomized inter trial intervals between 10-50s (90 to

697 120dB with 10 dB steps, 40ms duration with 0ms onset and offset ramps). The

698 fan was opened during whole experiment to reduce external noise interference.

699 Eight repetitions were recorded for each sound intensities per each subject.

700

33

Data analysis

Charts were plotted by Prism 6 (GraphPad Software, San Diego, CA). All data are mean ± SEM or SD, as indicated in the figure legends. ANOVA tests were used to determine statistical significance (*$P < 0.05$, **$P < 0.01$, ***$P < 0.001$, ****$P < 0.0001$).

Acknowledgements

Author contributions

L.L. did gRNA design, construction, FACS and deep sequencing, tissue culture and injectoporation, mouse surgery and viral injection, behavioral test; K.L. did genome data mining; L-Z.Z. performed the cochlear culture and injectoporation, immunostaining and plasmid preparation; H-Q.H. did behavioral test and immunostaining data quantification; Q.H. performed the cochlear culture and injectoporation; S.L. did the hair-cell electrophysiology and behavioral data analysis; S-F.W., Y-Z.W., J.L., C-M.S., J-F.C., C-R.L., H-B.D., and J.L. provided necessary help; F-Y.C., Z-G.X., W-Z.S. and Q-W.S. supervised some of the experiments; L.L. and W.X. designed experiments, generated figures, and wrote the manuscript; W.X. supervised the project.

Reference

1   Cornu, T. I., Mussolino, C. & Cathomen, T. Refining strategies to translate genome editing to the clinic. *Nat Med* **23**, 415-423, doi:10.1038/nm.4313 (2017).

2   Cox, D. B., Platt, R. J. & Zhang, F. Therapeutic genome editing: prospects and challenges. *Nat Med* **21**, 121-131, doi:10.1038/nm.3793 (2015).

3   Komor, A. C., Kim, Y. B., Packer, M. S., Zuris, J. A. & Liu, D. R. Programmable editing of a target base in genomic DNA without double-

35

stranded DNA cleavage. *Nature* **533**, 420-424, doi:10.1038/nature17946 (2016).

4   Gaudelli, N. M. *et al.* Programmable base editing of A*T to G*C in genomic DNA without DNA cleavage. *Nature* **551**, 464-471, doi:10.1038/nature24644 (2017).

5   Nishida, K. *et al.* Targeted nucleotide editing using hybrid prokaryotic and vertebrate adaptive immune systems. *Science* **353**, doi:10.1126/science.aaf8729 (2016).

6   Suzuki, K. *et al.* Precise in vivo genome editing via single homology arm donor mediated intron-targeting gene integration for genetic disease correction. *Cell Res* **29**, 804-819, doi:10.1038/s41422-019-0213-0 (2019).

7   Yao, X. *et al.* Homology-mediated end joining-based targeted integration using CRISPR/Cas9. *Cell Res* **27**, 801-814, doi:10.1038/cr.2017.76 (2017).

8   Suzuki, K. *et al.* In vivo genome editing via CRISPR/Cas9 mediated homology-independent targeted integration. *Nature* **540**, 144-149, doi:10.1038/nature20565 (2016).

9   van Overbeek, M. *et al.* DNA Repair Profiling Reveals Nonrandom Outcomes at Cas9-Mediated Breaks. *Mol Cell* **63**, 633-646, doi:10.1016/j.molcel.2016.06.037 (2016).

10   Allen, F. *et al.* Predicting the mutations generated by repair of Cas9-

36

induced double-strand breaks. *Nat Biotechnol*, doi:10.1038/nbt.4317 (2018).

11   Chakrabarti, A. M. *et al.* Target-Specific Precision of CRISPR-Mediated Genome Editing. *Mol Cell*, doi:10.1016/j.molcel.2018.11.031 (2018).

12   Shen, M. W. *et al.* Predictable and precise template-free CRISPR editing of pathogenic variants. *Nature*, doi:10.1038/s41586-018-0686-x (2018).

13   Leenay, R. T. *et al.* Large dataset enables prediction of repair after CRISPR-Cas9 editing in primary T cells. *Nat Biotechnol* **37**, 1034-1037, doi:10.1038/s41587-019-0203-2 (2019).

14   Koike-Yusa, H., Li, Y., Tan, E. P., Velasco-Herrera Mdel, C. & Yusa, K. Genome-wide recessive genetic screening in mammalian cells with a lentiviral CRISPR-guide RNA library. *Nat Biotechnol* **32**, 267-273, doi:10.1038/nbt.2800 (2014).

15   Iyer, S. *et al.* Precise therapeutic gene correction by a simple nuclease-induced double-stranded break. *Nature*, doi:10.1038/s41586-019-1076-8 (2019).

16   Shearer, A. E. & Smith, R. J. Genetics: advances in genetic testing for deafness. *Curr Opin Pediatr* **24**, 679-686, doi:10.1097/MOP.0b013e3283588f5e (2012).

17   Petit, C. Usher syndrome: from genetics to pathogenesis. *Annu Rev Genomics Hum Genet* **2**, 271-297, doi:10.1146/annurev.genom.2.1.271 (2001).

18   Alagramam, K. N. *et al.* The mouse Ames waltzer hearing-loss mutant is caused by mutation of Pcdh15, a novel protocadherin gene. *Nature genetics* **27**, 99-102 (2001).

19   Kazmierczak, P. *et al.* Cadherin 23 and protocadherin 15 interact to form tip-link filaments in sensory hair cells. *Nature* **449**, 87-91, doi:10.1038/nature06091 (2007).

20   Fu, Y., Sander, J. D., Reyon, D., Cascio, V. M. & Joung, J. K. Improving CRISPR-Cas nuclease specificity using truncated guide RNAs. *Nat Biotechnol* **32**, 279-284, doi:10.1038/nbt.2808 (2014).

21   Xiong, W., Wagner, T., Yan, L., Grillet, N. & Muller, U. Using injectoporation to deliver genes to mechanosensory hair cells. *Nat Protoc* **9**, 2438-2449, doi:10.1038/nprot.2014.168 (2014).

22   Platt, R. J. *et al.* CRISPR-Cas9 knockin mice for genome editing and cancer modeling. *Cell* **159**, 440-455, doi:10.1016/j.cell.2014.09.014 (2014).

23   Meyers, J. R. *et al.* Lighting up the senses: FM1-43 loading of sensory cells through nonselective ion channels. *Journal of Neuroscience* **23**, 4054-4065 (2003).

24   Pawlowski, K. S., Kikkawa, Y. S., Wright, C. G. & Alagramam, K. N. Progression of inner ear pathology in Ames waltzer mice and the role of protocadherin 15 in hair cell development. *J Assoc Res Otolaryngol* **7**, 83-94, doi:10.1007/s10162-005-0024-5 (2006).

25 Ashkenazy, H., Erez, E., Martz, E., Pupko, T. & Ben-Tal, N. ConSurf 2010: calculating evolutionary conservation in sequence and structure of proteins and nucleic acids. *Nucleic Acids Res* **38**, W529-533, doi:10.1093/nar/gkq399 (2010).

26 Hsu, P. D. *et al.* DNA targeting specificity of RNA-guided Cas9 nucleases. *Nat Biotechnol* **31**, 827-832, doi:10.1038/nbt.2647 (2013).

27 Symington, L. S. & Gautier, J. Double-strand break end resection and repair pathway choice. *Annu Rev Genet* **45**, 247-271, doi:10.1146/annurev-genet-110410-132435 (2011).

28 Akil, O. *et al.* Restoration of Hearing in the VGLUT3 Knockout Mouse Using Virally Mediated Gene Therapy. *Neuron* **75**, 283-293, doi:10.1016/j.neuron.2012.05.019 (2012).

29 Yu, Q. *et al.* Virally expressed connexin26 restores gap junction function in the cochlea of conditional Gjb2 knockout mice. *Gene Ther* **21**, 71-80, doi:10.1038/gt.2013.59 (2014).

30 Emptoz, A. *et al.* Local gene therapy durably restores vestibular function in a mouse model of Usher syndrome type 1G. *Proc Natl Acad Sci U S A*, doi:10.1073/pnas.1708894114 (2017).

31 Pan, B. *et al.* Gene therapy restores auditory and vestibular function in a mouse model of Usher syndrome type 1c. *Nat Biotechnol* **35**, 264-272, doi:10.1038/nbt.3801 (2017).

32 Nist-Lund, C. A. *et al.* Improved TMC1 gene therapy restores hearing

831 and balance in mice with genetic inner ear disorders. *Nat Commun* **10**,

832 236, doi:10.1038/s41467-018-08264-w (2019).

833 33 Akil, O. *et al.* Dual AAV-mediated gene therapy restores hearing in a

834 DFNB9 mouse model. *Proc Natl Acad Sci U S A* **116**, 4496-4501,

835 doi:10.1073/pnas.1817537116 (2019).

836 34 Gao, X. *et al.* Treatment of autosomal dominant hearing loss by in vivo

837 delivery of genome editing agents. *Nature*, doi:10.1038/nature25164

838 (2017).

839 35 Gyorgy, B. *et al.* Allele-specific gene editing prevents deafness in a

840 model of dominant progressive hearing loss. *Nat Med*,

841 doi:10.1038/s41591-019-0500-9 (2019).

842 36 Yeh, W. H. *et al.* In vivo base editing restores sensory transduction and

843 transiently improves auditory function in a mouse model of recessive

844 deafness. *Sci Transl Med* **12**, doi:10.1126/scitranslmed.aay9101 (2020).

845 37 Murcia, C. L. & Woychik, R. P. Expression of Pcdh15 in the inner ear,

846 nervous system and various epithelia of the developing embryo.

847 *Mechanisms of Development* **105**, 163-166, doi:Doi 10.1016/S0925-

848 4773(01)00388-4 (2001).

849 38 Stenson, P. D. *et al.* Human Gene Mutation Database (HGMD): 2003

850 update. *Hum Mutat* **21**, 577-581, doi:10.1002/humu.10212 (2003).

851 39 Di Palma, F. *et al.* Mutations in Cdh23, encoding a new type of cadherin,

852 cause stereocilia disorganization in waltzer, the mouse model for Usher

40

853   syndrome type 1D. *Nature Genetics* **27**, 103-107 (2001).

854   40   Ran, F. A. *et al.* Genome engineering using the CRISPR-Cas9 system.

855   *Nat Protoc* **8**, 2281-2308, doi:10.1038/nprot.2013.143 (2013).

856   41   Yang, Y. X. *et al.* Improved calcium sensor GCaMP-X overcomes the

857   calcium channel perturbations induced by the calmodulin in GCaMP.

858   *Nature Communications* **9**, doi:10.1038/s41467-018-03719-6 (2018).

859   42   Clement, K. *et al.* CRISPResso2 provides accurate and rapid genome

860   editing sequence analysis. *Nature Biotechnology* **37**, 224-226,

861   doi:10.1038/s41587-019-0032-3 (2019).

862   43   Stemmer, M., Thumberger, T., Keyer, M. D., Wittbrodt, J. & Mateo, J. L.

863   CCTop: An Intuitive, Flexible and Reliable CRISPR/Cas9 Target

864   Prediction Tool. *Plos One* **10**, doi:10.1371/journal.pone.0124633 (2015).

865   44   Bae, S., Park, J. & Kim, J. S. Cas-OFFinder: a fast and versatile

866   algorithm that searches for potential off-target sites of Cas9 RNA-guided

867   endonucleases. *Bioinformatics* **30**, 1473-1475,

868   doi:10.1093/bioinformatics/btu048 (2014).

869   45   Ashkenazy, H., Erez, E., Martz, E., Pupko, T. & Ben-Tal, N. ConSurf 2010:

870   calculating evolutionary conservation in sequence and structure of

871   proteins and nucleic acids. *Nucleic Acids Research* **38**, W529-W533,

872   doi:10.1093/nar/gkq399 (2010).

873   46   Hsu, P. D. *et al.* DNA targeting specificity of RNA-guided Cas9 nucleases.

874   *Nature Biotechnology* **31**, 827-+, doi:10.1038/nbt.2647 (2013).

875   47   Yang, X. J. *et al.* Surgery-free video-oculography in mouse models:

876   enabling quantitative and short-interval longitudinal assessment of

877   vestibular function. *Neuroscience Letters* **696**, 212-218,

878   doi:10.1016/j.neulet.2018.12.036 (2019).

879   48   Stahl, J. S., van Alphen, A. M. & De Zeeuw, C. I. A comparison of video

880   and magnetic search coil recordings of mouse eye movements. *Journal*

881   *of Neuroscience Methods* **99**, 101-110, doi:Doi 10.1016/S0165-

882   0270(00)00218-1 (2000).

883

884

885

886

887

888

889 **Main figure and figure legends**
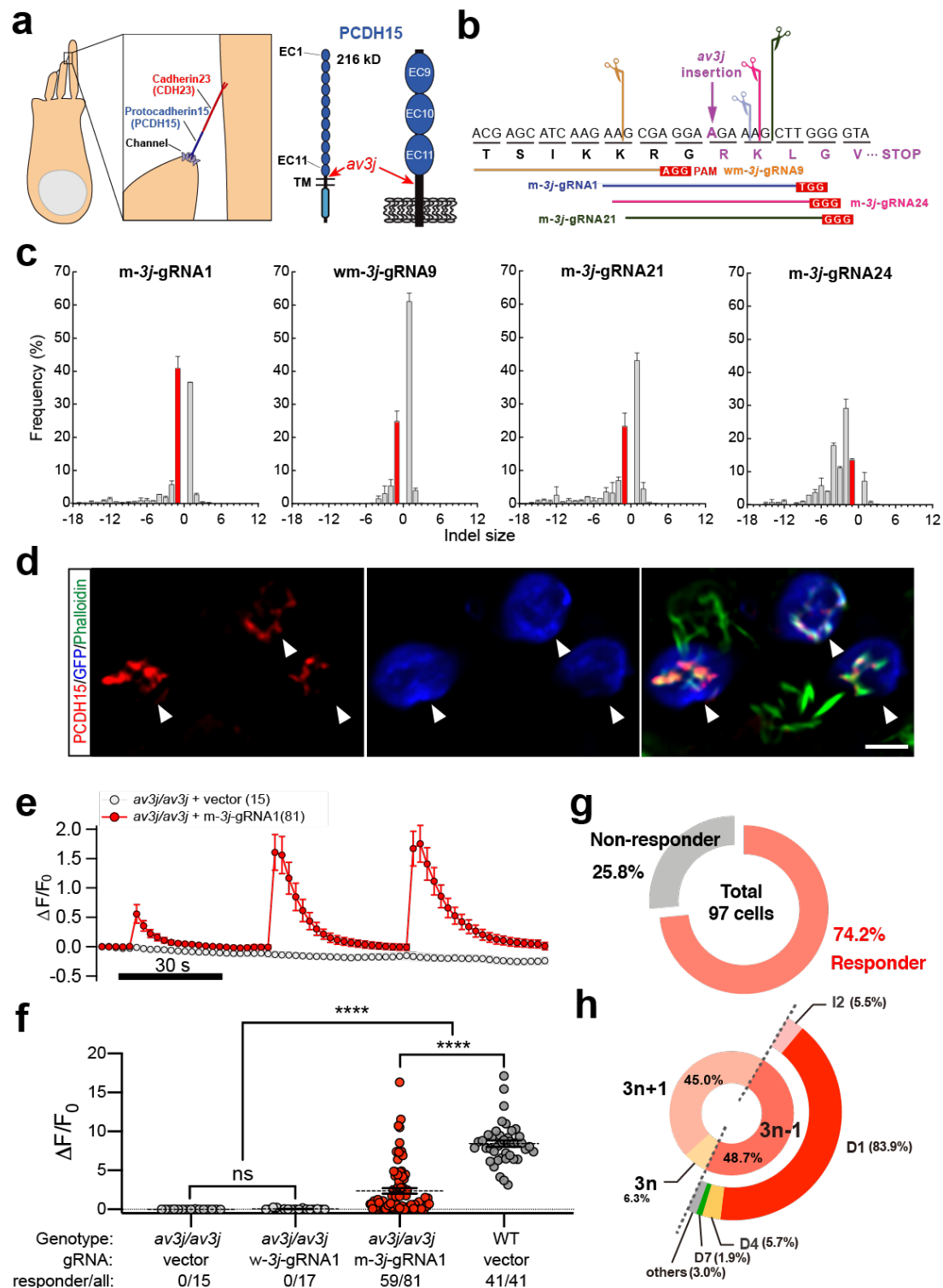
890

891

Fig. 1 | The selected m-*3j*-gRNA1 efficiently restores the *av3j* deficiency *ex vivo*.

a, PCDH15 is one of the two components of the tip link that gates the mechanotransduction channel in hair cells. The 216-kD PCDH15 contains 11 extracellular cadherin (EC) repeats and a transmembrane (TM) domain. The *av3j* mutation brings an A insertion between the EC11 and TM domain and causes an early stop codon in the *Pcdh15* gene. **b,** Four 17-nt gRNAs were designed to target the *av3j* A insertion site. The m-*3j*-gRNA1, m-*3j*-gRNA21, and m-*3j*-gRNA24 cover the insertion, while wm-*3j*-gRNA9 can target both wild-type (WT) and *av3j* alleles. **c,** The editing profiles of the 4 gRNAs shown as the indel frequency at each indel size. The bars of 1-bp deletion were highlighted in red, which was 40.9% for m-*3j*-gRNA1. Each gRNA profile had 2-3 replicates. Error bars, SD. **d,** PCDH15 protein immunostaining in the electroporated P3 *av3j/av3j* cochleae cultured for 2 days *in vitro* (P3+2DIV). PX330 containing m-*3j*-gRNA1 and Cas9 (PX330-m-*3j*-gRNA1) was co-electroporated with N1-EGFP. Note that only the hair bundles of electroporated *av3j/av3j* hair cells showed obvious signals (arrowhead). Scale bar, 3 μm. **e,** Averaged traces of Ca^{2+} responses activated by fluid-jet stimuli in *av3j/av3j* OHCs electroporated by control PX330 vector or PX330-m-*3j*-gRNA1 (P1+4 DIV). Error bars, SEM. **f,** Quantification of the maximal Ca^{2+} responses in OHCs from recordings similar to (**e**). W-*3j*-gRNA1 targets the corresponding WT sequence and shares the same PAM with m-*3j*-gRNA1. Responsive and total recorded cell numbers are shown in panels. Brown-Forsythe and Welch ANOVA test; ns, no significance, ****$P < 0.0001$, error bars, SEM. **g,** 74.2% (72/97) *av3j/av3j* auditory hair cells, including both OHCs (**f**) and IHCs (Supplementary Figure 1c), recovered mechanosensitivity after PX330-m-*3j*-gRNA1 electroporation. **h,** 48.7% editing products in m-*3j*-gRNA1 are '3n-1', which could restore the reading frame of *av3j*, and were dominated by 1-bp deletion (D1), 4-bp deletion (D4) and 2-bp insertion (I2) (See Supplementary Fig. 1d for details). Note that, correction of only one allele is sufficient to achieve a functional recovery of the diploid *av3j/av3j* hair cells.
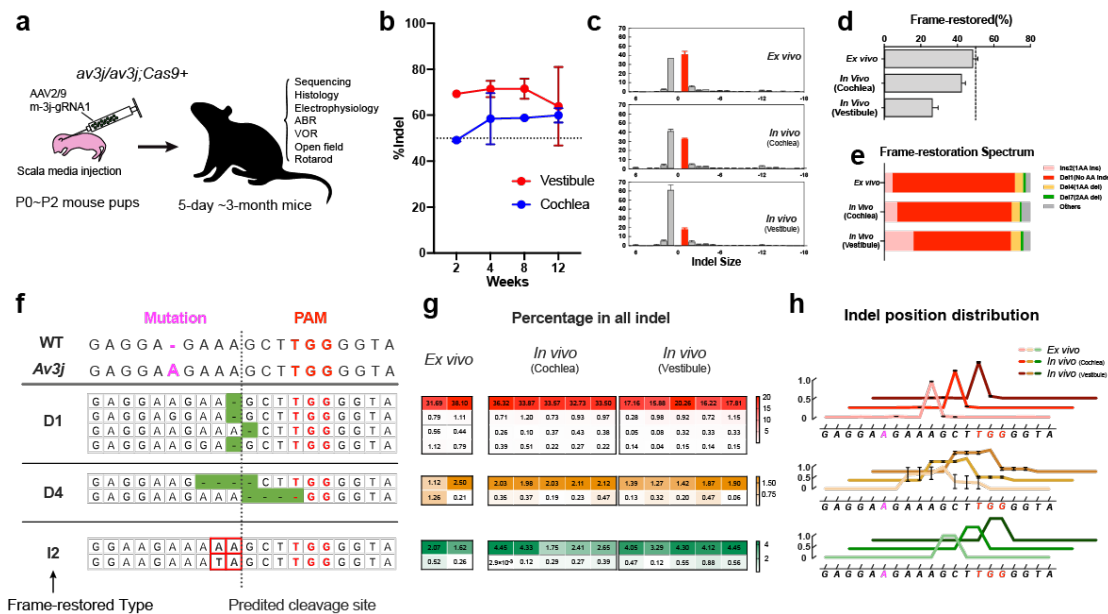
Fig. 2 | Similar editing outcomes of m-*3j*-gRNA1 *ex vivo* and *in vivo*.

a, A cartoon illustrating the overall procedures of *in vivo* gene delivery and evaluation in Fig. 2-4. AAV2/9-U6-m-*3j*-gRNA1-CMV-mCherry (0.8 µl, 1.5 × 10^{14} vg/ml) was injected to scala media of P0-P2 *av3j/av3j;Cas9+* mice bilaterally, followed by a variety of measurements at indicated ages. **b,** Genome editing efficiencies (quantified as indel percentage) in virus transfected cells of cochleae and vestibules. The tissues were harvested at age of 2, 4, 8, 12, 16 weeks post-viral delivery (PVD). The transfected cells were sorted by FACS then followed by deep sequencing (Supplementary Fig. 3a-d for details). Each group has 2-5 animals. **c-h,** Detailed editing product analysis of m-*3j*-g1 in electroporated cochlear cultures (P1+4DIV, *ex vivo*), AAV transfected cochleae and vestibules from *av3j/av3j;Cas9+* mice (1 month PVD, *in vivo*). Error bars, SD. **c,** The editing profiles of m-*3j*-gRNA1. Error bars, SD. **d,** The percentage of frame-restored editing product of m-*3j*-gRNA1. **e,** Frame-restoration spectrum analysis. **f,** The top three frame-restored types were dominant by 1-2 editing products. The mutant and WT sequence are shown on the top. *Av3j* mutation and PAM sequence are illustrated in magenta and red. The predicted Cas9 cleavage site is indicated by a dash line at 3bp upstream the NGG PAM. **g,** The percentage of the corresponding editing products in all indels, with each column indicating a single replicate. **h,** The indel position analysis. Color: lightest, cochleae *ex vivo*; medium, cochleae *in vivo*; darkest: vestibules *in vivo*. Error bars, SD.
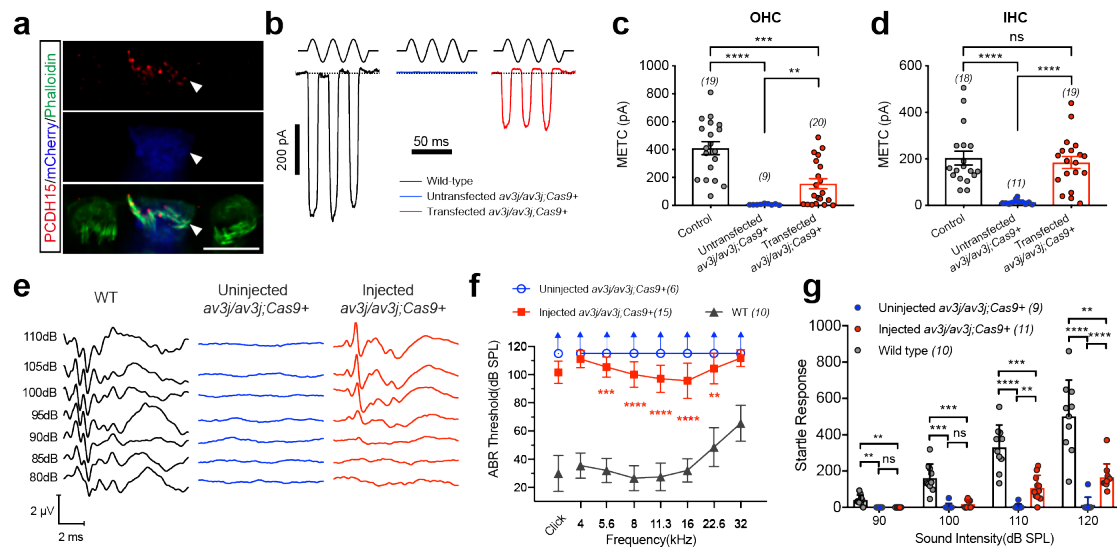
45

Fig. 3 | *In vivo* delivery of m-*3j*-gRNA1 ameliorates auditory symptom of *av3j/av3j;Cas9+* mice.

a, PCDH15 immunostaining (red) showing recovery of protein expression in the stereocilium tips in transfected OHCs (blue) from P0-P2 AAV injected *av3j/av3j;Cas9+* mice (tissue harvested 5 days PVD). Hair bundle were stained with phalloidin (green). Note that only the hair bundles of transfected *av3j/av3j* hair cells showed obvious signals (arrowhead). Scale bar, 6 μm. **b,** Representative examples of mechanotransduction currents recorded from OHCs in control and *av3j/av3j;Cas9+* mice with or without transfection (10 days PVD). A fluid jet was used to stimulate the hair bundle during recordings. **c-d,** Quantification of the mechanotransduction current amplitudes from recordings similar to (**b**) in OHCs (**c**) and IHCs (**d**). 14 out of 20 OHCs and 18 out of 19 IHCs were responsive. Littermate *av3j/+;Cas9+* or WT mice at the same age were used for control. **e,** Representative click ABR responses from 4-5 week WT, uninjected and injected *av3j/av3j;Cas9+* mice. **f,** Mean ABR thresholds in WT, uninjected and injected *av3j/av3j;Cas9+* mice. Statistics represented the difference between uninjected and injected *av3j/av3j;Cas9+* group. 15 out of 33 injected *av3j/av3j;Cas9+* mice recovered ABR responses. Only mice with ABR responses were plotted in the injected group. Arrows indicate the thresholds are higher than the maximal stimulus level. **g,** Startle responses to white noises were recorded in 4-5 week WT, uninjected and injected *av3j/av3j;Cas9+* mice. Only mice with startle responses were plotted in the injected group. 17 injected mice were tested in startle responses prior to ABR test, in which 11 had both startle and ABR recovery, 4 with ABR recovery only, and the rest 2 with no restoration in both tests. Brown-Forsythe and

975   Welch ANOVA test; error bars, SEM. ns, no significance, *$P < 0.05$, **$P <$
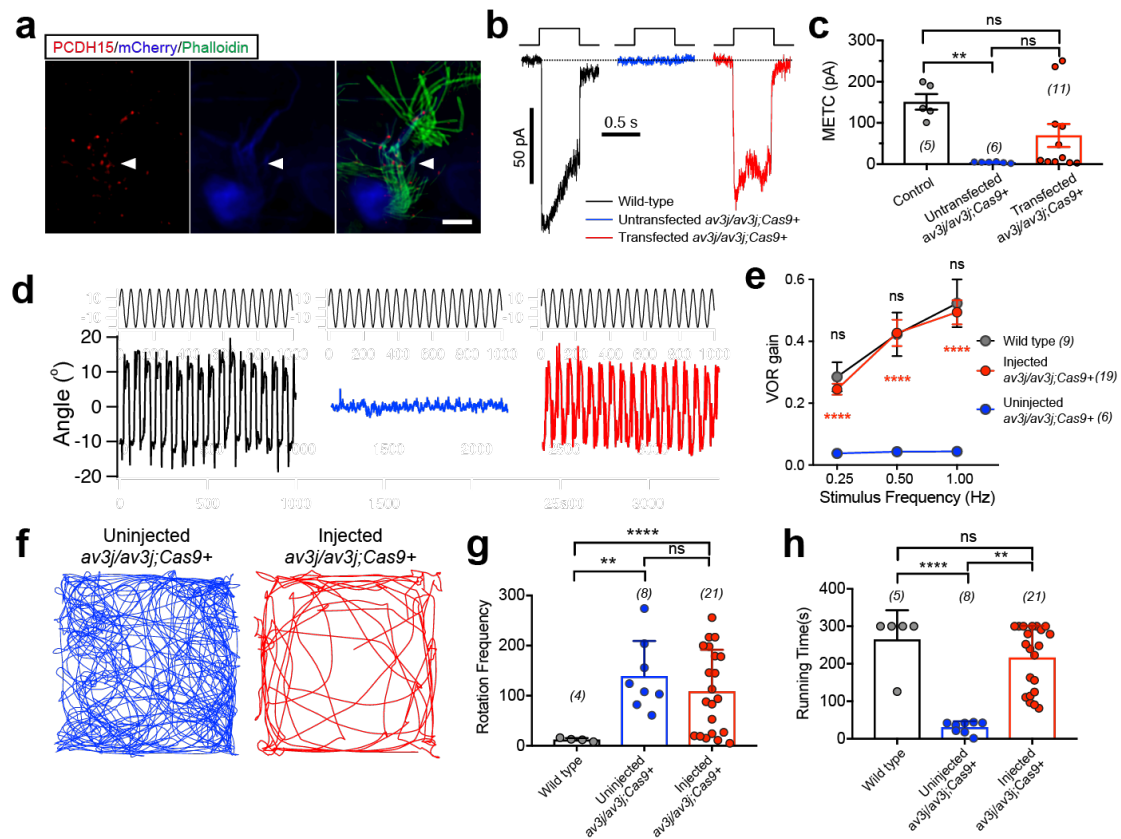
976   0.051, ***$P < 0.001$, ****$P < 0.0001$.

977

Fig. 4 | *In vivo* delivery of m-*3j*-gRNA1 ameliorates vestibular symptom of *av3j/av3j;Cas9+* mice.

a, PCDH15 protein expression (red) was recovered in the stereocilium tips of transfected vestibular hair cells (VHCs, blue) from injected *av3j/av3j;Cas9+* mice (10 days PVD). Hair bundle stained with phalloidin (green). Note that only the hair bundles of transfected *av3j/av3j* hair cells showed obvious signals (arrowhead). Scale bar, 3 μm. **b,** Representative examples of mechanotransduction currents recorded from VHCs in WT mice, uninjected and injected *av3j/av3j;Cas9+* mice (10 days PVD). A fluid jet was used for stimulation. **c,** Quantification of the mechanotransduction current amplitudes from recordings similar to (**b**). For transfected *av3j/av3j;Cas9+* VHCs, 7 out of 11 (64%) were responsive. P10 WT were used for positive control. **d,** Representative traces of VOR responses from WT mice, uninjected and injected *av3j/av3j;Cas9+* mice. **e,** Quantification of the VOR gain. Note that the responses of injected animals show no difference with WT mice in all frequencies. Statistics result between WT and injected group are shown in grey, injected vs uninjected shown in red. **f,** Examples of open-field locomotion traces of uninjected *av3j/av3j;Cas9+* littermates and injected *av3j/av3j;Cas9+* mice. **g,** Quantification of circling frequencies during open field tests. 7 out of 21 injected

48

998   mice had similar circling frequencies as WT, indicating a total recovery of the

999   circling symptom. **h,** Quantification of the running time in rotarod test obtained

1000   in WT mice, uninjected and injected *av3j/av3j;Cas9+* mice. Brown-Forsythe and

1001   Welch ANOVA test; ns, no significance, **P* < 0.01, ***P* < 0.001, ****P* < 0.0001;
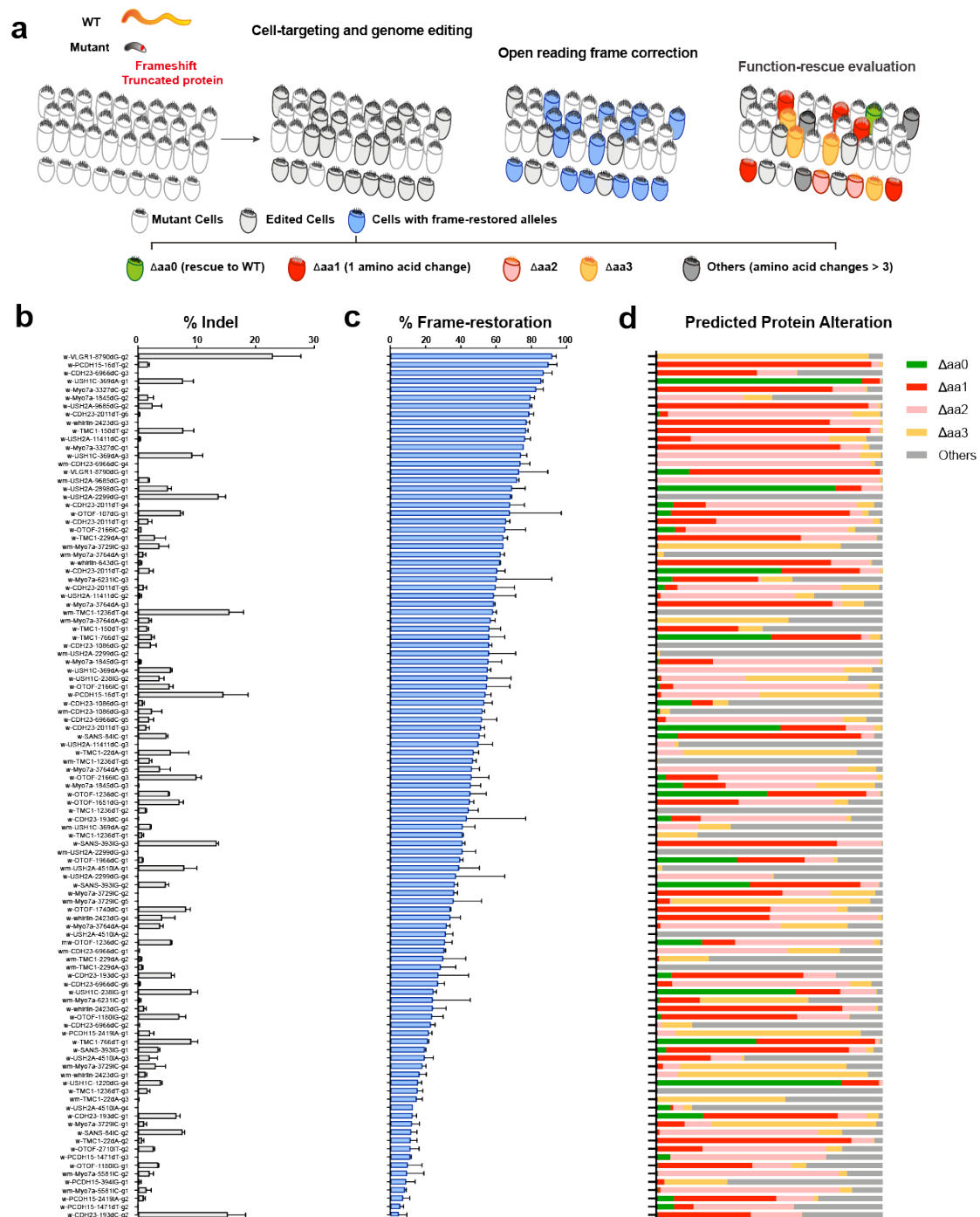
1002   error bars, SEM.

1003

1004

Fig. 5 | Editing outcome evaluation of 114 designed gRNAs targeting other frameshift deafness mutations.
a, Cartoon showing multiple factors relevant for frame-restoration gRNA evaluation: genome editing efficiency, frame-restoration ratios, and editing product function-rescue evaluation. **b,** Genome editing efficiencies of designed gRNAs, in which the %Indel data come from N2a cell line 72h post transfection of gRNA-carrying PX330 plasmid for it was difficult to tightly control the percentage of electroporated tissue cells throughout FACS sorting.

50

1013   **c,** The percentage of predicted frame-restored products of designed gRNAs.

1014   **d,** The predicted protein alteration spectrums after genome editing of each

1015   gRNA based on deep sequencing data from electroporated tissues. Color

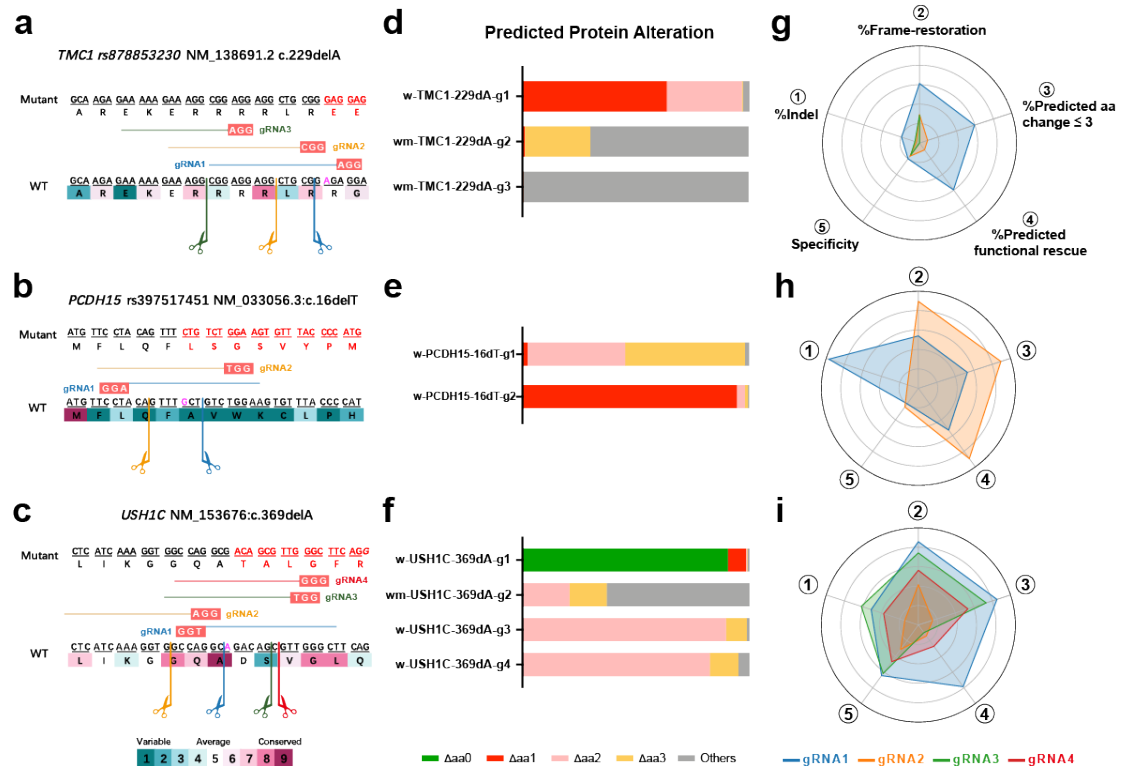1016   code indicates the number of amino acid changes relative to WT.

1017

Fig. 6 | Evaluation and selection of therapeutic gRNAs targeting other frameshift deafness mutations.

a-c, Therapeutic gRNA design for *TMC1* c.229delA (**a**), *PCDH15* c.16delT (**b**) and *USH1C* c.369delA (**c**). Magenta in WT indicate the mutant nucleotides, and frameshift sequences are colored in red in mutant sequences. The open reading frames are illustrated by underlines, and amino acids are colored by conservation levels, highly variable (deep green), highly conserved (muddy purple). The dash line showed the predicted cleavage site of each gRNA. **d-f,** The predicted protein alteration spectrum of gRNAs targeting *TMC1* c.229delA (**d**), *PCDH15* c.16delT (**e**) and *USH1C* c.369delA (**f**). **g-i,** Radar plots incorporating multiple parameters relevant for frame restoration to help gRNA evaluation and selection, as shown by gRNAs targeting *TMC1* c.229delA (**g**), *PCDH15* c.16delT (**h**) and *USH1C* c.369delA (**i**).

52